Distribution Grid Optimal Power Flow Integrating Volt-Var Droop of Smart Inverters

Alper Savasci, Adedoyin Inaolaji, and Sumit Paudyal
Florida International University, Miami, USA.

***Abstract*—Smart inverters (SIs) with local volt-var droop functions are effective in maintaining voltage and reactive power on the distribution feeders. Volt-var optimization (VVO) is generally carried out using distribution grid optimal power flow (DOPF)-based model that provides set point for the inverters and/or legacy grid devices. However, the existing works do not consider volt-var droop settings in the VVO framework, making the inverter dispatch solutions unsuitable at the local inverter controller level. Therefore, in this work, we propose the inclusion of SIs' local volt-var droop functions (as per the IEEE-1547) as constraints in the VVO formulation. We adopt a well-known second-order cone programming (SOCP) version of DOPF and with the inclusion of SIs' droop functions, the resulting VVO renders an efficient mixed-integer SOCP (MISOCP) problem. The efficacy of the proposed model is shown on a 33-node distribution feeder with 4 SIs having volt-var droop functions set as per the IEEE-1547.**

***Index Terms*—Distribution grid modeling, smart inverter, optimal power flow, volt-var, droop, second-order cone**

I. Introduction

Large-scale deployment of distributed photovoltaic (PV) generation in active distribution networks (ADN) brings both operational challenges and opportunities to the system operations. The potential impacts that PV could have on distribution systems is studied extensively in the literature [1]. The foremost technical issue with the incorporation of PVs on distribution networks is the voltage rise due to significant active power injection [2]. Traditionally, distribution feeder voltage is maintained by legacy devices including fixed/switched capacitor banks, load-tap changers and voltage regulators, which operate at a slow timescale [3], [4]. However, these legacy devices tend to make excessive switching operations to cope with rapid voltage fluctuations caused by high PV penetration, resulting in wear and tear associated with the degradation of the devices [5].

An alternative to the use of these legacy devices for dealing with fast voltage fluctuations is to utilize the active and reactive power injection/absorption capability of the distributed PVs through the control of the inverters. Smart inverters (SI) are power electronic devices with a capability to not only convert active DC power to AC power but also to inject and absorb reactive power. This reactive power support from the inverters is becoming indispensable for the economic operation of the ADN, as the reactive power support from the inverters help to reduce active power curtailment from the PVs to mitigate over voltage issues on the feeders.

Volt-var optimization (VVO) is an advanced function that distribution system operator routinely uses to dispatch the active and reactive power set points of dispatchable PVs with (or without) the control of legacy grid devices to optimally manage the voltage and reactive power profile on the distribution networks. In this context, the VVO can be cast as a distribution grid optimal power flow (DOPF) problem. Centralized DOPF-based VVO schemes have been proposed in [6], [7], where the inverter reactive power set points are determined centrally and dispatched to the inverters. In [8], a DOPF model and solution method considering the control of legacy devices and SIs are considered. A distributed VVO coordinating PV inverter dispatch is proposed in [9]. In [10], different shapes of P-Q capability curve of the inverters are integrated to a DOPF model. While the optimal inverter dispatch, as in [6]–[10], is an important problem to consider, the SIs should operated based on the local droops as defined in the IEEE-1547 [11]. Thus, the dispatch solution obtained from the methods as in [6]–[10], may not lie on the local droop settings of the SIs, which makes the DOPF-based solution unsuitable at the local inverter controller level. Moreover, the set points obtained from [6]–[10] may violate the interconnection standards.

Although there has been recent interest in modelling volt-var droop functionalities, i.e., $\mathbf{Q}(\mathbf{V})$, and determining their optimal settings [12], [13], these works are mainly focused on designing the optimal configurations of the $\mathbf{Q}(\mathbf{V})$ and no work exists in the literature that assesses the performance of the $\mathbf{Q}(\mathbf{V})$ integrated VVO in a network-wide optimization framework. Integration of $\mathbf{Q}(\mathbf{V})$ droop function within an DOPF framework is challenging as the DOPF in its original form is nonlinear and nonconvex problem, and $\mathbf{Q}(\mathbf{V})$ also being nonconvex brings additional computational challenges. In addition, the existing convex DOPF formulations mostly use square of voltage magnitude terms or product of voltage variables, while $\mathbf{Q}(\mathbf{V})$ modeling requires first-order voltage as an argument. One can propose to utilize fully-linearized DOPF formulations, which uses first order voltage term, as a base DOPF model; however, linearized DOPF formulations are obtained by ignoring the nonlinear loss term, which limits its usefulness for loss optimization type of studies. Considering the recent literature, integrating the mathematical model of $\mathbf{Q}(\mathbf{V})$ to an efficient convex DOPF framework is likely to have advantages in terms of improving the computational and

This work is supported in part by National Science Foundation grant ECCS-2001732. Corresponding Author: Alper Savasci, Florida International University, Email: asava014@fiu.edu.

modeling accuracy for $\mathbf{Q}(\mathbf{V})$ droop integrated DOPF.

This paper presents an efficient DOPF model that incorporates SIs' $\mathbf{Q}(\mathbf{V})$ droop settings as constraints of the DOPF problem. The two major challenges in the proposed approach are: the integration of piecewise droop functions of SIs in the DOPF formulation, and approximation of first order voltage term from the squared of the voltage magnitude used in the convex DOPF formulation. We propose to use a novel mixed-integer linear reformulation of piecewise $\mathbf{Q}(\mathbf{V})$ droop settings. The mixed-integer $\mathbf{Q}(\mathbf{V})$ model is then integrated as constraints to a well-known second-order cone programming (SOCP) version of the DOPF model. The first order voltage approximation is tested with five different approximation methods. The resulting formulation then becomes mixed-integer SOCP (MISOCP). We adopted SOCP DOPF as underlying base model and formulated the proposed model as MISOCP, as MISOCP is computationally more tractable than mixed-integer non-linear programming (MINLP) counter part [14], while mixed-integer linear programming (MILP) exhibits large errors on the solution accuracy [15].

The structure of this paper is organized as follows. Section II describes the mathematical model of volt-var droop of SIs. Section III presents the base DOPF model used in this study. Section IV explains the proposed approximation methods. Section V presents the volt-var integrated DOPF model. Section VI presents the case studies. Conclusion and future work are summarized in Section VII.

II. Modeling of Volt-Var Droop Settings

A. Reactive Power Capability of Smart Inverters

SIs can help improve PV hosting capacity of a feeder by controlling the reactive power. Thus, oversizing the inverter allows room for the inverter to produce inductive or capacitive reactive power as needed. Fig. 1 illustrates the reactive power capability of an inverter. With an apparent power rating (S_{rating}) that is greater than the real power rating (P_{rating}) of the inverter, the PV systems would have the capability of injecting (capacitive) /absorbing (inductive) reactive power even if the PVs are operated at the maximum active power rating.

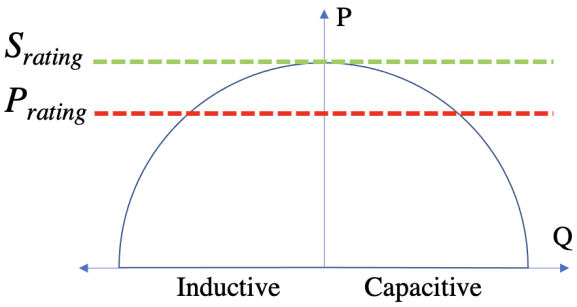

Fig. 1. Reactive Power Capability of SIs.

B. Piecewise Linear Model of Volt-Var Droop Settings

The volt-var curve is modelled as piecewise linear function, operating in full capacitive mode at low voltages and full inductive mode at high voltages, with a slope that describes the rate of change of the reactive power output with respect to change in the voltage at the point of connection of the PV. The curve centers around the nominal voltage with a dead band region in the middle. Fig. 2 depicts a typical SI's $\mathbf{Q}(\mathbf{V})$ curve with five piecewise linear segments. Depending on the configuration of the break points, the available operating range of the voltage is partitioned into multiple segments which define the reactive power control actions of the SIs within maximum inductive and capacitive reactive power available.

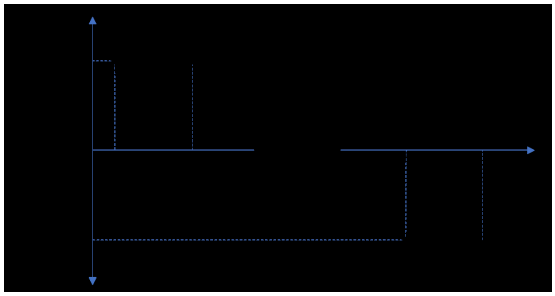

Fig. 2. A typical 5-segment $\mathbf{Q}(\mathbf{V})$ droop curve of SIs [11], [16].

In order to integrate the $\mathbf{Q}(\mathbf{V})$ droop curve of SIs into the DOPF framework, it has to be modelled analytically. Thus, one can utilize elegant integer-linear modelling techniques to model the piecewise linear nature of $\mathbf{Q}(\mathbf{V})$. The mathematical representation of $\mathbf{Q}(\mathbf{V})$ droop curve can be written as the following piecewise function,

$$Q_i(V_i) = \begin{cases} +Q_i^{\max}, & V_i^l \le V_i \le V_{i,2} \\ \frac{-Q_i^{\max}}{V_{i,3}-V_{i,2}} V_i + \frac{Q_i^{\max} V_{i,3}}{V_{i,3}-V_{i,2}}, & V_{i,2} < V_i \le V_{i,3} \\ 0, & V_{i,3} < V_i \le V_{i,4} \\ \frac{-Q_i^{\max}}{V_{i,5}-V_{i,4}} V_i + \frac{Q_i^{\max} V_{i,4}}{V_{i,5}-V_{i,4}}, & V_{i,4} < V_i \le V_{i,5} \\ -Q_i^{\max}, & V_{i,5} < V_i \le V_i^u \end{cases} \quad (1)$$

where i represents the node index to which SI is connected; V_i denotes the voltage at node i whose lower and upper bounds are given as V_i^l and V_i^u respectively. $V_{i,2}$ through $V_{i,5}$ are the break points of voltage V_i. $Q_i^{\max}$ is the maximum reactive power rating of the SI. The active segment with respect to the node voltage V_i can be selected through the use of binary variables, i.e., $\delta_{i,1}, \ldots, \delta_{i,5} \in \{0,1\}$, and $Q_i(V_i)$ function can be collectively written as,

$$\begin{aligned} Q_i(V_i) = {} & \delta_{i,1}\ (+Q_i^{\max}) \\ & + \delta_{i,2} \left(\frac{-Q_i^{\max}}{V_{i,3}-V_{i,2}} V_i + \frac{Q_i^{\max} V_{i,3}}{V_{i,3}-V_{i,2}} \right) \\ & + \delta_{i,3}\ (0) \\ & + \delta_{i,4} \left(\frac{-Q_i^{\max}}{V_{i,5}-V_{i,4}} V_i + \frac{Q_i^{\max} V_{i,4}}{V_{i,5}-V_{i,4}} \right) \\ & + \delta_{i,5}\ (-Q_i^{\max}) \end{aligned} \quad (2)$$

where only one binary variable has to be activated to enable one segment of $Q_i(V_i)$, while disabling the other segments. This is achieved by enforcing the following logical constraint,

$$\sum_{m=1}^{5} \delta_{i,m} = 1 \tag{3}$$

Using big-M modelling approach [17], the binary variables are combined with the lower bound, upper bound, and break points of voltage on each segment of $Q_i(V_i)$, which is enforced with the following set of inequalities,

$$\left.\begin{aligned} -(1-\delta_{i,1})\ M + V_i^l \ &\leq V_i \leq\ V_{i,2} + (1-\delta_{i,1})\ M \\ -(1-\delta_{i,2})\ M + V_{i,2} \ &\leq V_i \leq\ V_{i,3} + (1-\delta_{i,2})\ M \\ -(1-\delta_{i,3})\ M + V_{i,3} \ &\leq V_i \leq\ V_{i,4} + (1-\delta_{i,3})\ M \\ -(1-\delta_{i,4})\ M + V_{i,4} \ &\leq V_i \leq\ V_{i,5} + (1-\delta_{i,4})\ M \\ -(1-\delta_{i,5})\ M + V_{i,5} \ &\leq V_i \leq\ V_i^u + (1-\delta_{i,5})\ M \end{aligned}\right\} \tag{4}$$

Although the set of equations (2)-(4) defines the piecewise nature of the $Q_i(V_i)$ curve, (2) is nonlinear because of the bilinear terms, which are products of binary variable δ_i and continuous variable V_i, particularly for the 2^{nd} and 4^{th} segments where the $Q_i(V_i)$ curve has slope. Hence, we apply an exact linearization method to the bilinear terms in (2). Consider two new variables $W_{i,2} := \delta_{i,2}\, V_i$ and $W_{i,4} := \delta_{i,4}\, V_i$. Then, (2) is reformulated as following,

$$\begin{aligned} Q(V_i) = &\delta_{i,1}\ (Q_i^{\max}) \\ &+ W_{i,2}\left(\frac{-Q_i^{\max}}{V_{i,3}-V_{i,2}}\right) + \delta_{i,2}\left(\frac{Q_i^{\max} V_{i,3}}{V_{i,3}-V_{i,2}}\right) \\ &+ \delta_{i,3}\,(0) \\ &+ W_{i,4}\left(\frac{-Q_i^{\max}}{V_{i,5}-V_{i,4}}\right) + \delta_{i,4}\left(\frac{Q_i^{\max} V_{i,4}}{V_{i,5}-V_{i,4}}\right) \\ &+ \delta_{i,5}\ (-Q_i^{\max}) \end{aligned} \tag{5}$$

where new variables are coupled with existing segment bounds with a modified set of inequalities as,

$$\left.\begin{aligned} -(1-\delta_{i,1})\ M + V_i^l \leq V_i \leq V_{i,2} + (1-\delta_{i,1})\ M \\ -M\ (1-\delta_{i,2}) \leq V_i - W_{i,2} \leq (1-\delta_{i,2})\ M \\ V_{i,2}\,\delta_{i,2} \leq W_{i,2} \leq V_{i,3}\,\delta_{i,2} \\ -(1-\delta_{i,3})\ M + V_{i,3} \leq V_i \leq V_{i,4} + (1-\delta_{i,3})\ M \\ -M\ (1-\delta_{i,4}) \leq V_i - W_{i,4} \leq (1-\delta_{i,4})\ M \\ V_{i,4}\,\delta_{i,4} \leq W_{i,4} \leq V_{i,5}\,\delta_{i,4} \\ -(1-\delta_{i,5})\ M + V_{i,5} \leq V_i \leq V_i^u + (1-\delta_{i,5})\ M \end{aligned}\right\} \tag{6}$$

Equations (3), (5), and (6) define the analytical integer-linear $\mathbf{Q}(\mathbf{V})$ droop curve representation.

III. Base Distribution Grid OPF Model

We use the well-known branch power flow based second-order cone relaxation [18] version of distribution OPF model (SOCP-DOPF). A radial distribution network can be represented as a directed graph, $\mathcal{G} = (\mathcal{N}, \mathcal{E})$, where $\mathcal{N}$ is node set and $\mathcal{E}$ is the branch set. The SOCP-DOPF can be mathematically formulated as,

$$\underset{P_g, Q_g, u_i, \ell_i}{\operatorname{argmin}} \ \sum\nolimits_{(i,j)\in\mathcal{E}}\ r_{ij}\ell_{ij} \tag{7}$$

Subject to :

$$p_j^g - p_j^d = \sum_{k:(j,k)\in\mathcal{E}} P_{jk} - \sum_{i:(i,j)\in\mathcal{E}} (P_{ij} - r_{ij}\ell_{ij}), \quad \forall j \in \mathcal{N} \tag{8}$$

$$q_j^g - q_j^d = \sum_{k:(j,k)\in\mathcal{E}} Q_{jk} - \sum_{i:(i,j)\in\mathcal{E}} (Q_{ij} - x_{ij}\ell_{ij}), \quad \forall j \in \mathcal{N} \tag{9}$$

$$v_j = v_i - 2\left(r_{ij}P_{ij} + x_{ij}Q_{ij}\right) + \left(r_{ij}^2 + x_{ij}^2\right)\ell_{ij}, \quad \forall (i,j) \in \mathcal{E} \tag{10}$$

$$\left\| \begin{matrix} 2P_{ij} \\ 2Q_{ij} \\ \ell_{ij} - v_i \end{matrix} \right\|_2 \leq \ell_{ij} + v_i, \qquad \forall (i,j) \in \mathcal{E} \tag{11}$$

$$0 \leq p_i^g \leq P^{\text{PV}}, \qquad \forall i \in \mathcal{N}_{\text{PV}} \tag{12}$$

$$0 \leq p_i^g \leq S_i^{\max}, \qquad \forall i \in \mathcal{N}_{\text{PV}} \tag{13}$$

$$-S_i^{\max} \leq q_i^g \leq S_i^{\max}, \qquad \forall i \in \mathcal{N}_{\text{PV}} \tag{14}$$

$$(p_i^g)^2 + (q_i^g)^2 \leq (S_i^{\max})^2, \qquad \forall i \in \mathcal{N}_{\text{PV}} \tag{15}$$

$$p_j^g \in [p_j^{g,l},\, p_j^{g,u}],\ \ q_j^g \in [q_j^{g,l},\ \ q_j^{g,u}],\ \ \forall j \in \mathcal{N}' \setminus \mathcal{N}_{\text{PV}} \tag{16}$$

$$v_j \in [v_j^l,\, v_j^u], \qquad \forall j \in \mathcal{N}' \tag{17}$$

where i, j indicate nodes on the feeder. v_i is the magnitude squared node voltage, i.e., $v_i = |V_i|^2$ and ℓ_{ij} is magnitude squared of branch current, i.e., $\ell_{ij} = |I_i|^2$. p_j^g (q_j^g) and p_j^d (q_j^d) are the real (reactive) power generation and demand respectively at node j. P_{ij} and Q_{ij} represent the sending-end real and reactive power respectively flowing on the line (i,j). $\mathcal{N}'$ is the set of nodes excluding the substation node. $\mathcal{N}_{\text{PV}}$ represents the nodes which have PV generation.

In the formulation, (7) denotes the objective function in the form of total active power loss, nodal real and reactive power balance are given by (8) and (9) respectively, voltage drop equations for each line segment is given by (10). Second-order cone constraint is given by (11), which relates the node voltage and branch current with branch power flow variables. (12) and (13) define the limits on PV generation based on the solar irradiance and inverter apparent power rating. The reactive injection/absorption limit is defined by (14). The coupling between real and reactive power output of inverter is defined by convex constraint (15). The real and reactive generation limits are set by (16) at non-PV nodes, 0-upper and 0-lower bounds are enforced for the buses which do not have any generation. Voltage bounds are defined in (17).

IV. First Order Voltage Approximation

The main challenge in integrating $Q_i(V_i)$ in the base SOCP-DOPF is that the droop settings in $Q_i(V_i)$ uses the first order of voltage magnitude V_i, whereas the base SOCP-DOPF model uses squared of the voltage magnitude, i.e., v_i. Hence, the relationship of $v_i = V_i^2$ needs to be modelled in the DOPF formulation when the $Q_i(V_i)$ curve is integrated to the base SOCP-DOPF model. However, enforcing this quadratic relationship as a constraint makes the overall formulation nonlinear in nature and defeats the purpose of using base

SOCP-DOPF model. Since the $Q_i(V_i)$ formulation as in (3), (5), and (6) require integer variables to model, so then the natural choice would be to formulate the resulting DOPF model as a MISOCP formulation. Thus, reformulating constraint $v_i = V_i^2$ as linear or mixed-integer linear constraint would fit with the modeling structure of the MISOCP.

Next, we explain five approximation methods to represent $v_i = V_i^2$ in linear or mixed-integer linear form in order to combine base SOCP-DOPF model with the $\mathbf{Q}(\mathbf{V})$ droop model.

A. Taylor Series Expansion (TSE)

The quadratic voltage relationship can be approximated by Taylor series expansion around an operating point a as following,

$$v_i = a^2 + 2a(V_i - a) + (V_i - a)^2, \quad \forall i \in \mathcal{N}_{\text{PV}} \tag{18}$$

where $a \in [V_i^l, V_i^u]$. If the quadratic term in (18) is ignored, it can be approximated as the following linear model,

$$\langle V_i^2 \rangle^{TSE} \equiv a^2 + 2a(V_i - a), \quad \forall i \in \mathcal{N}_{\text{PV}} \tag{19}$$

where the elimination of quadratic term leads to an error whose value depends on the choice of parameter a.

B. McCormick Relaxation (M)

The standard McCormick relaxation, also known as McCormick envelopes [19], provides a linear relaxation of a bilinear term. In this approach, the general bilinear term $x_i\, x_j$ is replaced with a new variable w_{ij}, and the formal relation of the new variable and the existing variables are constructed with a set of four linear inequalities.

The magnitude squared term in SOCP-DOPF model can be viewed as a bilinear ($v_i = V_i^2 = V_i\, V_i$) term and can be relaxed using the standard McCormick relaxation as following,

$$\langle V_i^2 \rangle^{M} \equiv \begin{cases} v_i \geq V_i^l\, V_i + V_i^l\, V_i - V_i^l\, V_i^l \\ v_i \geq V_i^u\, V_i + V_i^u\, V_i - V_i^u\, V_i^u \\ v_i \leq V_i^l\, V_i + V_i^u\, V_i - V_i^l\, V_i^u \\ v_i \leq V_i^u\, V_i + V_i^l\, V_i - V_i^u\, V_i^l \end{cases}, \forall i \in \mathcal{N}_{\text{PV}} \tag{20}$$

where the first two inequalities are underestimators while the last two are the overestimators. Depending on the types of the variables in bilinear term, it is possible to have less number of inequalities. For example, in this particular case of representation the overestimators are duplicating. Hence, only one overestimator is sufficient.

C. Piecewise McCormick Relaxation (PW-M)

The standard McCormick relaxations might not always provide tight convex envelope representation. Hence, the concept of piecewise McCormick relaxation via partition-dependent bounds has been proposed in [20]–[22] to obtain tighter convex envelop computation, which leads to improved accuracy compared to the standard McCormick relaxation. In order to strengthen the relaxation, the available range of the variable(s) (x^l, x^u) in the bilinear term $x_i\, x_j$ can be partitioned into N segments. The partitioning can be done for one of the variables (univariate) or both variables (bivariate), uniformly or non-uniformly. In this study, we choose to use bivariate piecewise McCormick relaxation via uniform partitioning, which results in the following mixed-integer formulation,

$$\langle V_i^2 \rangle^{PW-M} \equiv \begin{cases} v_i \geq \sum_{n=1}^{\text{N}} \big(V_{in}^l\, V_{in} + V_{in}^l\, V_{in} - V_{in}^l\, V_{in}^l y_{in} \big) \\ v_i \geq \sum_{n=1}^{\text{N}} \big(V_{in}^u\, V_{in} + V_{in}^u\, V_{in} - V_{in}^u\, V_{in}^u y_{in} \big) \\ v_i \leq \sum_{n=1}^{\text{N}} \big(V_{in}^l\, V_{in} + V_{in}^u\, V_{in} - V_{in}^l\, V_{in}^u y_{in} \big) \\ v_i \leq \sum_{n=1}^{\text{N}} \big(V_{in}^u\, V_{in} + V_{in}^l\, V_{in} - V_{in}^u\, V_{in}^l y_{in} \big) \end{cases} \quad \forall i \in \mathcal{N}_{\text{PV}} \tag{21}$$

$$\sum\nolimits_{n=1}^{\text{N}} y_{in} = 1, \qquad \forall i \in \mathcal{N}_{\text{PV}} \tag{22}$$

$$V_{in}^l\, y_{in} \leq V_{in} \leq V_{in}^u\, y_{in}, \quad \forall n \in \{1, \ldots, \text{N}\}, \forall i \in \mathcal{N}_{\text{PV}} \tag{23}$$

$$V_i = \sum\nolimits_{n=1}^{\text{N}} V_{in}, \qquad \forall i \in \mathcal{N}_{\text{PV}} \tag{24}$$

$$V_{in}^l = V_i^l + \frac{(V_i^u - V_i^l)\,(n-1)}{\text{N}}, \quad \forall n \in \{1, \ldots, \text{N}\}, \forall i \in \mathcal{N}_{\text{PV}} \tag{25}$$

$$V_{in}^u = V_i^l + \frac{(V_i^u - V_i^l)\, n}{\text{N}}, \ \forall n \in \{1, \ldots, \text{N}\}, \forall i \in \mathcal{N}_{\text{PV}} \tag{26}$$

where V_{in} denotes the variable for partition n, which can only take values within partition bounds $[V_{in}^l, V_{in}^u]$, binary variable $y_{in} \in \{0, 1\}$ denotes the status of the each partition whether it is enabled (binary-1) or disabled (binary-0), (21) defines under- and over-estimators as a sum of mixed-integer linear form, (22) ensures only one partition will be enabled, (23) constraints the value of each partition variable, enabled partition variable is coupled with the variable V_i by (24). Equations (25) and (26) set partition lower and upper bounds, respectively.

D. Quadratic Relaxation (QR)

The magnitude squared voltage term can be relaxed using its convex envelope as in [23], which can be represented mathematically using two linear inequality constraints as,

$$\langle V_i^2 \rangle^{QR} \equiv \begin{cases} v_i \geq V_i^2 \\ v_i \leq \big(V_i^u + V_i^l \big)\, V_i - V_i^u V_i^l \end{cases} \quad \forall i \in \mathcal{N}_{\text{PV}} \tag{27}$$

E. Piecewise Quadratic Relaxation (PW-QR)

Similar to the piecewise McCormick relaxation, piecewise version of QR can be derived as following,

$$\langle V_i^2 \rangle^{PW-QR} \equiv \begin{cases} v_i \geq \sum_{n=1}^{\text{N}} V_{in}^2 \\ v_i \leq \sum_{n=1}^{\text{N}} \big(\big(V_{in}^u + V_{in}^l \big)\, V_{in} - V_{in}^u V_{in}^l y_{in} \big) \end{cases} \quad \forall i \in \mathcal{N}_{\text{PV}} \tag{28}$$

$$\text{Equations (22) - (26)} \tag{29}$$

The formulated approximation models can be collected in the set $\mathcal{A} = \{TSE,\, M\,, PW\text{–}M\,, QR\,, PW\text{–}QR\}$.

V. Volt-var integrated DOPF

A DOPF model integrating base SOCP-DOPF model and $\mathbf{Q}(\mathbf{V})$ droop model of SIs is formulated as,

$$\underset{\substack{p_i^g, q_i^g, P_{ij}, Q_{ij}, u_i, \ell_{ij}, \\ V_i, V_{in}, y_{in}, W_{ik}, \delta_{ik}}}{\text{argmin}} \quad \sum\nolimits_{(i,j)\in\mathcal{E}} r_{ij}\ell_{ij} \tag{30}$$

Subject to :

Constraints (8) - (17) (31)

SI droop model : (3), (5), (6) , $\forall i \in \mathcal{N}_{\text{PV}}$ (32)

Approximation model $\in \mathcal{A}$, $\forall i \in \mathcal{N}_{\text{PV}}$ (33)

$y_{in} \in \{0,1\}, \quad \forall n \in \{1,\ldots,\text{N}\}, \forall i \in \mathcal{N}_{\text{PV}}$ (34)

$\delta_{ik} \in \{0,1\}, \quad \forall k \in \{1,\ldots,5\}, \forall i \in \mathcal{N}_{\text{PV}}$ (35)

The above formulation is MISOCP in nature.

VI. Case Studies

A. Test Feeder

Simulations are carried out on a modified 33-node feeder [24] shown in Fig. 3. In the network, 4 PV generation sites of 1.5 MVA each are connected to the MV feeder through the smart inverters equipped with $\mathbf{Q}(\mathbf{V})$ droop functionality. We use the same line parameters and peak loads as the original network in [24]. We further generate time-series load profiles for each node by properly scaling the peak loads. The total time-series load and PV generation profiles used for the simulations are shown in Fig. 4.

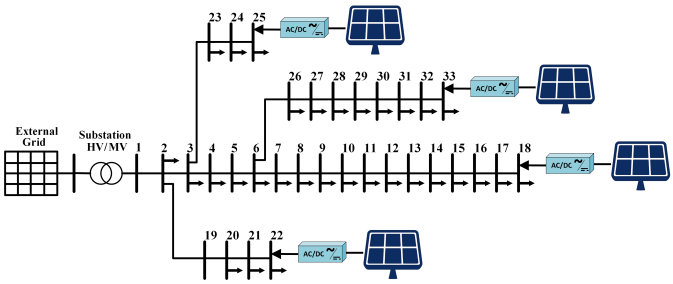

Fig. 3. Modified 33-node [24] feeder with 4 PV generation sites.

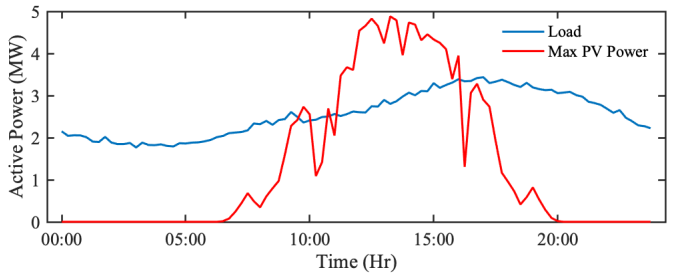

Fig. 4. Time-series load and PV generation profile.

A MacOS based machine with core-i5 2.9 GHz processor and 8 GB of RAM is used to carry out the simulations. Gurobi is chosen as an optimization solver and 0.01% of optimality gap limit is set in the solver.

B. Evaluation of Accuracy of First Order Voltage Approximation Methods

We compare the accuracy of the first order voltage approximation proposed in Section IV. The $\mathbf{Q}(\mathbf{V})$ integrated DOPF formulation given by (30)-(35), is solved for every 15-min (96 intervals in total for one day) with each voltage approximation model in $\mathcal{A}$. Since the formulation has two decision variables $\sqrt{v_i}$ and V_i, for the PV connected nodes, the approximation model used introduces some amount of error in the solution. The difference between $\sqrt{v_i}$ and V_i can be quantified with the average relative error calculated over all the PV connected nodes for daily simulation as following,

$$e_t = \frac{1}{|\mathcal{N}_{\text{PV}}|} \sum_{i\in\mathcal{N}_{\text{PV}}} \left| \frac{\sqrt{v_i^t} - V_i^t}{\sqrt{v_i^t}} \right| 100\ (\%), \forall t \in \mathcal{T} \tag{36}$$

where t denotes the time interval index, and $\mathcal{T} = \{1,\ldots,96\}$ represents the time interval index set. Furthermore, we obtain a compact error metric by averaging all e_t over the optimization horizon as,

$$Err = \frac{1}{\mathcal{T}} \sum_{t\in\mathcal{T}} e_t \tag{37}$$

In the simulation, we consider $V_i^l = 0.9$ and $V_i^u = 1.1$ p.u. Taylor series parameter is set to $a = (V_i^l + V_i^u)/2$. We consider two sets of voltage break points: {0.9, 0.92, 0.95, 0.96, 1.05, 1.1} p.u. and {0.9, 0.92, 0.98, 1.02, 1.08, 1.1} p.u. in $Q_i(V_i)$ droops. We use 7 uniform voltage segments for PW-M and PW-QR. $Q_i^{\max}$ is set to 1.5 MVAr. Table I and II summarize the average approximation errors for each methods in $\mathcal{A}$ for the two $\mathbf{Q}(\mathbf{V})$ droop configurations. The piecewise methods (i.e., PW-M and PW-QR) result in less errors compared to other approaches; however, both piecewise approaches are not dominating each other as the approximation accuracy is also dependent on the $\mathbf{Q}(\mathbf{V})$ droop configuration, i.e., the break points.

TABLE I
Average Approximation Errors (%) of each method in $\mathcal{A}$, $\mathbf{Q}(\mathbf{V})$ Configuration of {0.9, 0.92, 0.95, 0.96, 1.05, 1.1} p.u.

TSE	M	QR	PW-M	PW-QR
0.06	0.42	0.45	0.0042	0.0045

TABLE II
Average Approximation Errors (%) of each method in $\mathcal{A}$ $\mathbf{Q}(\mathbf{V})$ Configuration of {0.9, 0.92, 0.98, 1.02, 1.08, 1.1} p.u.

TSE	M	QR	PW-M	PW-QR
0.03	0.46	0.41	0.0067	0.0048

Fig. 5 and Fig. 6 show the accuracy of the proposed approaches on the voltage at node-25 for the corresponding droop configurations. It can be observed that piecewise relaxations provide good approximation between $\sqrt{v_i}$ and V_i, compared to the non piecewise methods. Note that Taylor series expansion can also provide decent approximation

accuracy considering it requires less number of variables and no integer variables to approximate V_i from v_i.

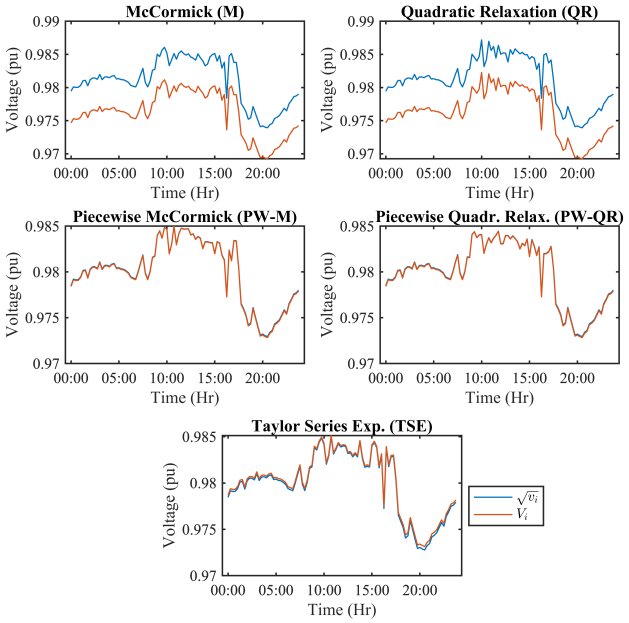

Fig. 5. Comparison of voltage approximation performance at node-25 with $\mathbf{Q}(\mathbf{V})$ configuration of {0.9, 0.92, 0.95, 0.96, 1.05, 1.1}p.u.

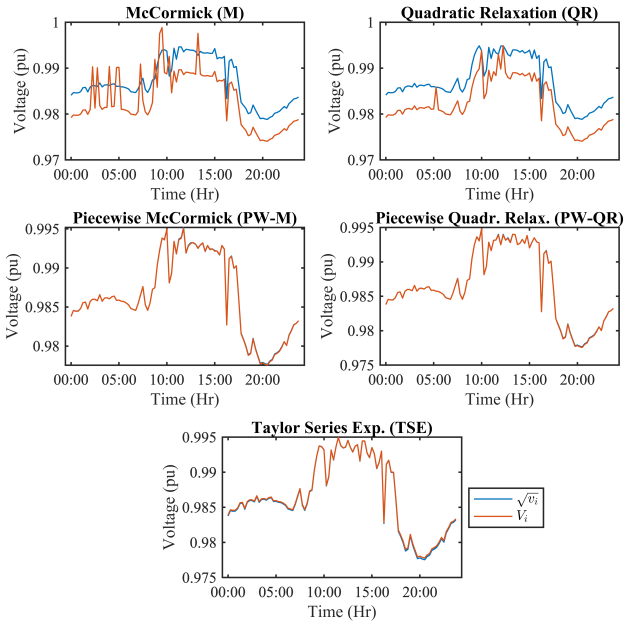

Fig. 6. Comparison of voltage approximation performance at node-25 with $\mathbf{Q}(\mathbf{V})$ configuration of {0.9, 0.92, 0.98, 1.02, 1.08, 1.1}p.u.

C. Comparison of Loss Reduction Performance

The loss reduction performance is highly dependent on the configuration of $\mathbf{Q}(\mathbf{V})$ droop settings. Tables III and IV show average active power loss values over 96-interval for two different $\mathbf{Q}(\mathbf{V})$ droop curve configurations with proposed approximation approaches. It can be observed that non-piecewise relaxations (M and QR) result in lower loss values for both droop configurations; however, considering their poor voltage approximation accuracy from Tables I and II, it reveals that there is an obvious trade off between loss reduction and voltage approximation accuracy for these methods.

Average power loss reduction performance of TSE and piecewise relaxation approaches (PW-M and PW-QR) result in close loss values for both droop configurations although the piecewise relaxations are slightly better in loss reduction performance. Among piecewise relaxations PW-QR marginally outperforms PW-M.

TABLE III
AVERAGE POWER LOSS (KW) BY EACH METHOD IN $\mathcal{A}$, WITH $\mathbf{Q}(\mathbf{V})$ CONFIGURATION OF {0.9, 0.92, 0.95, 0.96, 1.05, 1.1}P.U.

TSE	M	QR	PW-M	PW-QR
78.97	72.45	72.39	77.85	77.72

TABLE IV
AVERAGE POWER LOSS (KW) BY EACH METHOD IN $\mathcal{A}$ WITH $\mathbf{Q}(\mathbf{V})$ CONFIGURATION OF {0.9, 0.92, 0.98, 1.02, 1.08, 1.1}P.U.

TSE	M	QR	PW-M	PW-QR
48.04	45.32	45.65	47.74	47.68

D. Reactive Power Dispatch on $\mathbf{Q}(\mathbf{V})$ Droop

Next we present the effectiveness of the mixed-integer reformulation of $\mathbf{Q}(\mathbf{V})$ droops and how the reactive power dispatch solution using proposed DOPF model (30) - (35) lies on the $\mathbf{Q}(\mathbf{V})$ droops. The results presented in this part are obtained by using PW-QR approximation as it provides more accurate voltage performance over other proposed methods. Fig. 7 and 8 show the reactive power dispatch values (for 96-intervals and 4 PVs) and the $\mathbf{Q}(\mathbf{V})$ droops. The dispatch solutions in both figures exactly follow the mathematical model of the droop settings. Unlike the DOPF models in [6]–[10], our proposed approach abide the IEEE-1547.

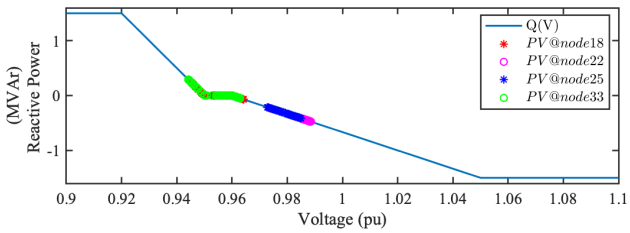

Fig. 7. Comparison of reactive dispatch and $\mathbf{Q}(\mathbf{V})$ droop with configuration of {0.9, 0.92, 0.95, 0.96, 1.05, 1.1}p.u.

Fig. 9 and Fig. 10 provide more insights on the accuracy of the solution. The reactive power dispatch obtained by the proposed DOPF and the reactive power calculated by plugging in the voltage solution into the $\mathbf{Q}(\mathbf{V})$ droops match for both $\mathbf{Q}(\mathbf{V})$ configurations.

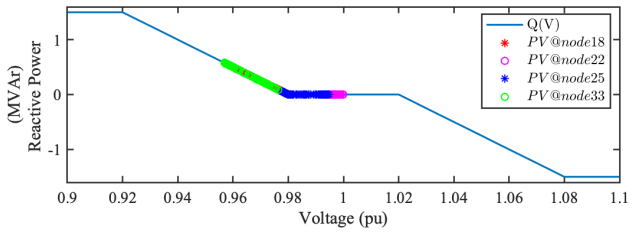

Fig. 8. Comparison of reactive dispatch and $\mathbf{Q}(\mathbf{V})$ droop with voltage configuration {0.9, 0.92, 0.98, 1.02, 1.08, 1.1}p.u.

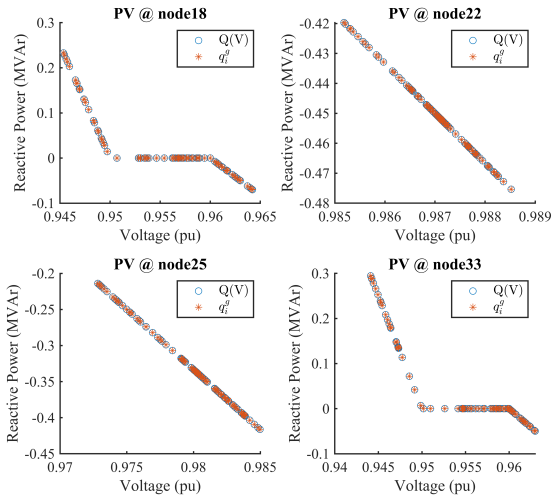

Fig. 9. Reactive power dispatch with $\mathbf{Q}(\mathbf{V})$ droop of {0.9, 0.92, 0.95, 0.96, 1.05, 1.1}p.u.

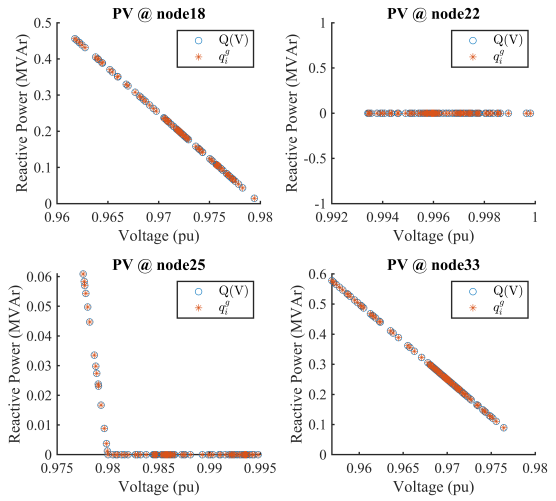

Fig. 10. Reactive power dispatch with $\mathbf{Q}(\mathbf{V})$ droop of {0.9, 0.92, 0.98, 1.02, 1.08, 1.1}p.u.

E. Computational Performance of $\mathbf{Q}(\mathbf{V})$ Droop Integrated DOPF

Fig. 11 shows the statistical properties of solution time for each time interval obtained using the various approximation method. It can be observed that DOPF for all intervals can be solved in less than 0.4 sec by using each method. The piecewise relaxation methods (PW-M and PW-QR) tend to take more time compared to TSE and M as they include integer partition variables for voltage approximation in $\mathcal{A}$. However, solution time with QR appears to be more dispersed compared to the other methods. Table V summarizes the number of continuous and integer variables required to build the model for each voltage approximation method in $\mathcal{A}$.

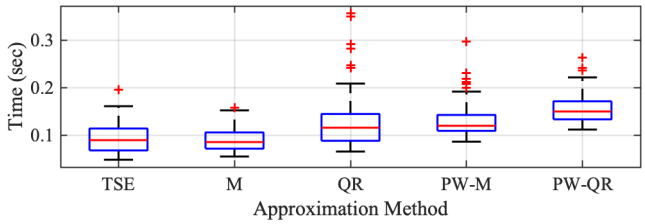

Fig. 11. Solution time of $\mathbf{Q}(\mathbf{V})$ integrated DOPF.

TABLE V
NUMBER OF CONTINUOUS AND INTEGER VARIABLES USED IN EACH VOLTAGE APPROXIMATION METHOD IN $\mathcal{A}$.

Method in $\mathcal{A}$	Continuous Variables	Integer Variables
TSE	207	20
M	207	20
QR	207	20
PW-MC	235	48
PW-QR	235	48

F. Tightness of the Solutions

Tightness is an important characteristic measure of accuracy of the solutions which can be evaluated as the error on branch flows, i.e., $\Delta S_{ij}^2 = |P_{ij}^2 + Q_{ij}^2 - \ell_{ij} v_i|$. The smaller value means the solution is tighter. Since $\mathbf{Q}(\mathbf{V})$ droop integrated DOPF is based on underlying SOCP relaxation, the tightness evaluation with each voltage approximation method in $\mathcal{A}$ gives an idea how accurate the solution is (not to be confused with the optimality gap set in the solver). Fig. 12 shows the tightness evaluations over the each branch for each voltage approximation method in $\mathcal{A}$, which is obtained less than 1.5×10^{-5}. This means the obtained solutions are tight.

VII. Conclusion and Future Work

This paper presented a volt-var droop integrated DOPF for optimal dispatch of smart inverters in active distribution networks. The proposed DOPF model is an MISOCP, which is based on well known BFM-based SOCP-DOPF and exact mixed-integer linear formulation of volt-var droop curve of smart inverters. In addition, we proposed a set of approximation methods to couple the first order voltage term used in volt-var droop model to the squared voltage magnitude used in SOCP-DOPF model. The adopted MISOCP formulation is tested on a modified 33-node feeder with proposed approximation methods in terms of approximation (coupling) accuracy, power loss reduction, and computational

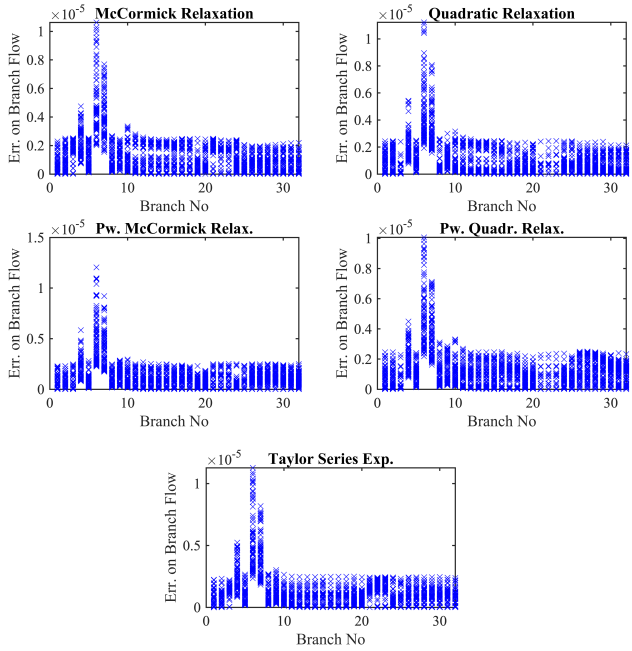

Fig. 12. Tightness evaluation of $\mathbf{Q}(\mathbf{V})$ droop integrated DOPF.

performance. We showed that the proposed mathematical model is tractable and can provide good quality solutions, which makes the model promising for practical-sized feeders. The proposed model can readily be combined with an optimization framework which configure not only the volt-var droop functionality of the smart inverters but also volt-watt and $\mathbf{P}(\mathbf{Q})$ droop as defined in the IEEE-1547. Hence, the proposed droop-integrated DOPF model can further improve loss reduction and voltage performance. As a future work, we are working on testing the scalability of the proposed method on larger networks and designing a dynamic optimization framework of optimal volt-var droop settings in order to obtain the best individual droop configuration of each smart inverters for daily operation.

REFERENCES

[1] J. Jung, A. Onen, K. Russell, and R. P. Broadwater, "Local steady-state and quasi steady-state impact studies of high photovoltaic generation penetration in power distribution circuits," *Renewable and Sustainable Energy Reviews*, vol. 43, pp. 569–583, 2015.

[2] P. M. S. Carvalho, P. F. Correia, and L. A. F. M. Ferreira, "Distributed reactive power generation control for voltage rise mitigation in distribution networks," *IEEE Transactions on Power Systems*, vol. 23, no. 2, pp. 766–772, 2008.

[3] J. J. Grainger and S. Civanlar, "Volt/var control on distribution systems with lateral branches using shunt capacitors and voltage regulators Part I: The overall problem," *IEEE Transactions on Power Apparatus and Systems*, vol. PAS-104, no. 11, pp. 3278–3283, 1985.

[4] S. L. Purucker, R. J. Thomas, and L. D. Monteen, "Feeder automation designs for installing an integrated distribution control system," *IEEE Transactions on Power Apparatus and Systems*, vol. PAS-104, no. 10, pp. 2929–2934, 1985.

[5] B. Palmintier, J. Giraldez, K. Gruchalla, P. Gotseff, A. Nagarajan, T. Harris, B. Bugbee, M. Baggu, J. Gantz, and E. Boardman, "Feeder voltage regulation with high-penetration pv using advanced inverters and a distribution management system: A duke energy case study," tech. rep., National Renewable Energy Lab. (NREL), USA, 2016.

[6] M. Farivar, R. Neal, C. Clarke, and S. Low, "Optimal inverter var control in distribution systems with high pv penetration," in *Proc. IEEE Power and Energy Society General Meeting*, pp. 1–7, 2012.

[7] X. Su, M. A. Masoum, and P. J. Wolfs, "Optimal PV inverter reactive power control and real power curtailment to improve performance of unbalanced four-wire LV distribution networks," *IEEE Transactions on Sustainable Energy*, vol. 5, no. 3, pp. 967–977, 2014.

[8] Q. Nguyen, H. V. Padullaparti, K.-W. Lao, S. Santoso, X. Ke, and N. Samaan, "Exact optimal power dispatch in unbalanced distribution systems with high pv penetration," *IEEE Transactions on Power Systems*, vol. 34, no. 1, pp. 718–728, 2018.

[9] Q. Zhang, K. Dehghanpour, and Z. Wang, "Distributed CVR in unbalanced distribution systems with PV penetration," *IEEE Transactions on Smart Grid*, vol. 10, no. 5, pp. 5308–5319, 2018.

[10] S. Karagiannopoulos, C. Mylonas, P. Aristidou, and G. Hug, "Active distribution grids providing voltage support: The swiss case," *IEEE Transactions on Smart Grid*, 2020.

[11] "IEEE standard for interconnection and interoperability of distributed energy resources with associated electric power systems interfaces," *IEEE Std 1547-2018 (Revision of IEEE Std 1547-2003)*, pp. 1–138, 2018.

[12] H. Lee, J.-C. Kim, and S.-M. Cho, "Optimal volt–var curve setting of a smart inverter for improving its performance in a distribution system," *IEEE Access*, vol. 8, pp. 157931–157945, 2020.

[13] A. O'Connell and A. Keane, "Volt–var curves for photovoltaic inverters in distribution systems," *IET Generation, Transmission Distribution*, vol. 11, no. 3, pp. 730–739, 2017.

[14] S. R. Shukla, S. Paudyal, and M. R. Almassalkhi, "Efficient distribution system optimal power flow with discrete control of load tap changers," *IEEE Transactions on Power Systems*, vol. 34, no. 4, pp. 2970–2979, 2019.

[15] A. Inaolaji, A. Savasci, S. Paudyal, and S. Kamalasadan, "Accuracy of phase-decoupled and phase-coupled distribution grid power flow models," in *Proc. IEEE Innovative Smart Grid Technologies (North America)*, pp. 1–5, 2021.

[16] B. Seal and B. Ealey, "Common functions for smart inverters, version 3," *Electric Power Research Institute (EPRI)*, 2014.

[17] H. P. Williams, *Model building in mathematical programming*. John Wiley & Sons, 2013.

[18] M. Farivar and S. H. Low, "Branch flow model: Relaxations and convexification—Part I," *IEEE Transactions on Power Systems*, vol. 28, no. 3, pp. 2554–2564, 2013.

[19] G. P. McCormick, "Computability of global solutions to factorable nonconvex programs: Part I—convex underestimating problems," *Mathematical programming*, vol. 10, no. 1, pp. 147–175, 1976.

[20] M. F. Hasan and I. Karimi, "Piecewise linear relaxation of bilinear programs using bivariate partitioning," *AIChE journal*, vol. 56, no. 7, pp. 1880–1893, 2010.

[21] P. M. Castro, "Tightening piecewise mccormick relaxations for bilinear problems," *Computers & Chemical Engineering*, vol. 72, pp. 300–311, 2015.

[22] H. Nagarajan, M. Lu, E. Yamangil, and R. Bent, "Tightening mccormick relaxations for nonlinear programs via dynamic multivariate partitioning," in *Proc. International Conference on Principles and Practice of Constraint Programming*, pp. 369–387, Springer, 2016.

[23] H. Hijazi, C. Coffrin, and P. Van Hentenryck, "Convex quadratic relaxations for mixed-integer nonlinear programs in power systems," *Mathematical Programming Computation*, vol. 9, no. 3, pp. 321–367, 2017.

[24] M. E. Baran and F. F. Wu, "Network reconfiguration in distribution systems for loss reduction and load balancing," *IEEE Transactions on Power Delivery*, vol. 4, no. 2, pp. 1401–1407, 1989.